

Lamellar Phases in Nonuniform Electric Fields: Breaking the In-Plane Rotation Symmetry and the Role of Dielectric Constant Mismatch

Y. Tsori

Department of Chemical Engineering,

Ben Gurion University of the Negev,

Beer Sheva 84105, Israel.

Email: tsori@bgu.ac.il

(Dated: 28/1/2007)

We consider orientational transitions of lamellar phases under the influence of a spatially nonuniform electric field. The transition between parallel and perpendicular lamellar stackings with respect to the substrate is investigated as a function of the system parameters. The dielectrophoretic energy and the energy penalty for having dielectric interfaces perpendicular to the field's direction are identified as linear and quadratic terms in a free energy expansion in the dielectric constant mismatch. We find that if the dielectric constant mismatch $\Delta\epsilon$ is smaller than some critical value $\Delta\epsilon_c$, parallel lamellar stacking will be realized, no matter how large the voltage difference between electrodes is. At $\Delta\epsilon > \Delta\epsilon_c$, perpendicular stacking will appear if the voltage is high enough. Nonuniform fields remove the in-plane degeneracy present in the more common uniform fields. We therefore calculate the energy of grains of different orientations. The torque acting on the grains leads to the preference of only one orientation. The results have direct implications to block copolymer orientation and to surface patterning on the nanometer scale.

Introduction. In recent years we have seen a large effort directed toward finding ways to control the phase-behavior and orientation of self-assembled structures [1, 2]. Confinement between two solid surfaces [3, 4, 5, 6, 7, 8, 9, 10, 11, 12, 13], shear flow [14], or the use of external electric fields [15, 16, 17, 18, 19, 20, 21, 22, 23, 24, 25, 26, 27] have proved very useful. The use of electric fields is especially appealing, as the field strength scales favorably with the system size. Spatially uniform electric fields, however, pose a long-lasting problem since the orientation of the assembled phases is not unique – the symmetry of the field means that all grain rotations in the plane are energetically equivalent.

Spatially varying fields remove this degeneracy, and thus can be quite useful in alignment of various mesophases. The early experiments of Russell *et al.* [28] have employed nonuniform fields, but ever since then all research have been on uniform fields. It seems that now, when such spatially uniform fields have been well understood and exploited possibly to their full potential, it is time to come back to spatially varying fields. In this article we focus on the most simple periodic structure – the lamellar phase, which is found under the influence of an electric field emanating from a “razor-blade” electrode design (see Fig. 1). The lamellae are made up of two different materials, A and B, e.g., diblock copolymers. In this example, the two polymers A and B have different dielectric constants, ϵ_A and ϵ_B . In the following we assume ion-free polymers; alternatively, for ion-containing polymers, application of a quasi-static field in the frequency ~ 1 kHz renders the ions immobile but leaves the electrostatic equations unchanged [17]. In spatially uniform electric fields, the lowest-order contribution to the system electrostatic free energy is quadratic in the permittivity difference of the two constituents, $\Delta\epsilon \equiv \epsilon_A - \epsilon_B$. As is explained in detail below, an inhomogeneity of the field gives rise to a dielectrophoretic force which is manifested in a linear term in $\Delta\epsilon$, and this has significance to the orientation selection and to phase-transitions [29].

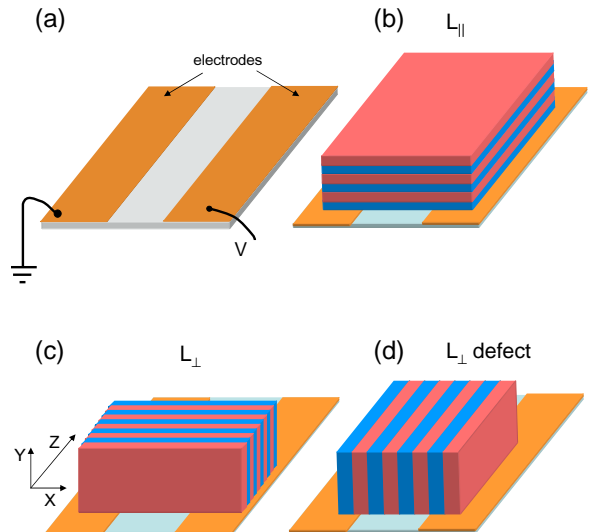


FIG. 1: Schematic illustration of the system. (a) Two thin “razor-blade” electrodes are laid down on the substrate. The voltage difference between them is V . (b) Parallel stacking L_{\parallel} – lamellae lie parallel to the substrate. (c) If the voltage is sufficiently high, electric field can overcome interfacial interactions and prefer a perpendicular stacking L_{\perp} (lamellae are parallel to the field lines). (d) A defect – an unfavorable perpendicular morphology where lamellae are perpendicular to the field lines. In subsequent calculations we took the distance between electrodes to be $1 \mu\text{m}$, and the lamellar period is 100 nm unless otherwise indicated.

At this point it should also be pointed out that nonuniform electric fields are in general neither interfacial nor purely bulk ones. In the razor-blade geometry, the field is high close to the electrodes' edge. However, sufficiently far from the electrodes the field behaves like $E(r) = V/\pi r$, where r is the distance from the middle of the gap. Thus, the integrated electrostatic contribution to the energy scales like $1/r$. This energy indeed decays, but very slowly, and it has an important contribution even very

far from the electrodes.

We assume that the lamellae are rigid enough so that the electric field does not bend them. In the example of block copolymers, this corresponds to the so-called strong-segregation regime, where $\chi N \gg 1$. Let us verify the validity of this assumption. The elastic bending energy per unit volume is written as $F_{\text{el}} = \frac{1}{2}K/R^2$, where K is the bending modulus, and R is the local bending radius (inverse curvature). For strongly stretched lamellae, $K = D\gamma_{AB}$, where D is the lamellar period ($D \sim 100$ nm) and $\gamma_{AB} \sim 10$ mN/m is the A/B interfacial tension. On the other hand, the electrostatic energy per unit volume is $F_{\text{es}} = \frac{1}{2}\epsilon E^2$, where ϵ is the dielectric constant and E the local field, which cannot exceed ~ 100 V/ μm because of dielectric breakdown. Let us take this maximum value, in this case $F_{\text{es}} = 10^5$ J/ m^3 . Therefore, $F_{\text{el}} = F_{\text{es}}$ if the lamellae are bent with a radius of curvature of $0.1 \mu\text{m}$. The same estimate relates to the stresses (forces) of course. Electric fields cannot bend lamellae to a radius smaller than $\sim 0.1 \mu\text{m}$. In the razor-blade system, at larger distances from the electrodes the field is weaker, and therefore the lamellae should stay flat as well. Since the fields we consider are typically much weaker, we do not expect bent lamellae in this electrode arrangement. The above reasoning does not hold for weakly segregated lamellae: These lamellae have a much weaker modulus K and therefore significant bending can occur.

A lamellar stack can therefore have the basic configurations: parallel or perpendicular to the substrate (Fig. 1 (b) and (c)), denoted as L_{\parallel} and L_{\perp} , respectively. Note that in the parallel stacking the first layer at the substrate is half as thick as the others. A third state exists which we denote the perpendicular defect. Here the lamellae normals are not parallel to the electrodes' edges. Fig. 1 (d) represents the highest energy of such defects. Weakly segregated systems exhibit lower energy defects, e.g., T-junction or grain boundary. In some experiments with weakly segregated block copolymers on preferential surfaces, few lamellar layers are adsorbed preferentially on the substrate (mixed morphology) due to the long-range effect of surface ordering [17, 30]. As is mentioned above, this system is out of the scope of the current work, and it will be dealt with in a subsequent publication.

A peculiar feature of nonuniform fields is that the L_{\parallel} state can be favored over the L_{\perp} one even in the absence of specific interfacial interactions with the substrate. In order to understand this, consider first the distribution of electric field squared for two semiinfinite planar electrodes in the x - z plane, with a gap of $1 \mu\text{m}$ between them. This distribution is shown in Fig. 2 for a medium with spatially uniform dielectric constant ϵ . Clearly E^2 is very high close to the surface and, in particular, close to the electrodes' edge at $x = \pm 0.5 \mu\text{m}$. The field is small far from the substrate, and therefore interfacial instabilities are not expected [31]; this is true even more so since above the electrodes' edges the field at $y \rightarrow \infty$ is actually parallel to the substrate and also to the polymer/air interface.

Let us now assume without loss of generality that $\epsilon_A > \epsilon_B$. As is well-known in the field of dielectrophoretic forces [32], a material with large value of ϵ is drawn to regions with high fields, whereas small- ϵ material is repelled.

Since the electric field is largest near the electrodes' edges, an L_{\parallel} state can form with the A-material touching the substrate. However, the work of Amundson *et al.* has shown that there is also a free energy penalty for having dielectric interfaces perpendicular to the field's direction, and this penalty is absent in the L_{\perp} state. Clearly, the orientation selection depends on the magnitude of $\epsilon_A - \epsilon_B$.

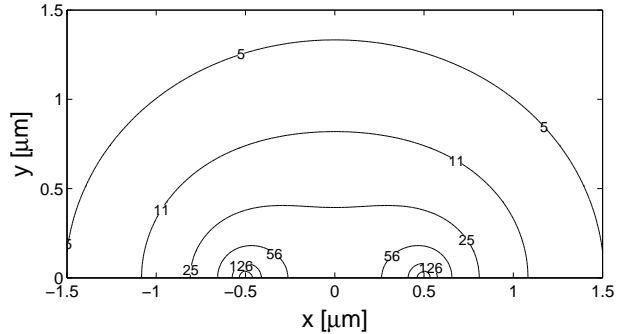


FIG. 2: Plot of $E^2(x, y)$ in the x - y plane, for the case where the dielectric constant ϵ is uniform, and the electrodes are at $x > 0.5 \mu\text{m}$ ($V = \frac{1}{2} \text{ V}$) and $x < -0.5 \mu\text{m}$ ($V = -\frac{1}{2} \text{ V}$). The largest field is at the electrodes' edge, $x = \pm 0.5 \mu\text{m}$. E^2 is scaled by 10^{10} and given in $(\text{V}/\text{m})^2$.

The electrostatic energy of the system is given by an integral over all space,

$$F_{\text{es}} = -\frac{1}{2} \int \epsilon(\mathbf{r}) \mathbf{E}^2(\mathbf{r}) \, d^3r \quad (1)$$

The dielectric constant $\epsilon(\mathbf{r})$ is a spatially varying quantity. In this study it is a periodic function. In the L_{\parallel} state, for example, it is given by

$$\epsilon(\mathbf{r}) = \begin{cases} \bar{\epsilon} + \frac{1}{2}\Delta\epsilon & \text{if } nd < y < nd + \frac{1}{2}d, \\ \bar{\epsilon} - \frac{1}{2}\Delta\epsilon & \text{if } nd + \frac{1}{2}d < y < (n+1)d, \end{cases} \quad n = 0, 1, 2, \dots \quad (2)$$

where $\bar{\epsilon} \equiv \frac{1}{2}(\epsilon_A + \epsilon_B)$ is the average dielectric constant, and the period is d . The above equation simply represents a square-wave in the y -direction, where ϵ alternates between ϵ_A and ϵ_B . The dielectric constant can be defined similarly for the other stackings.

Theory and Results. Figure 3 shows F_{es} for the L_{\parallel} and L_{\perp} stackings at a fixed value of $\bar{\epsilon} = 6$ and varying values of the dielectric constant mismatch. The electrostatic energy is calculated numerically for a system with electrode gap of $1 \mu\text{m}$. $F_{\text{es}}(\Delta\epsilon)$ (dashed horizontal line) is constant for the L_{\perp} case, because the electric field between the electrodes is independent of $\Delta\epsilon$ and $\bar{\epsilon}$. On the other hand, in the L_{\parallel} case (solid line), $F_{\text{es}}(\Delta\epsilon)$ decreases first before it increases. The decrease is due to the dielectrophoretic term, linear in $\Delta\epsilon$, while the increase is due to the penalty associated with dielectric interfaces perpendicular to the field lines, scaling like $(\Delta\epsilon)^2$.

Let us make a short but very general mathematical digression which will clarify the last point. Denote $\mathbf{E}_0(\mathbf{r})$

the electric field which corresponds to a system of uniform dielectric constant and a given electrode design (not necessarily the one in Fig. 1). \mathbf{E}_0 is derived from a potential $\psi_0(\mathbf{r})$ satisfying the proper boundary conditions on the electrodes: $\mathbf{E}_0 = -\nabla\psi_0$. Suppose now that the dielectric constant changes from its average value by an amount $\varepsilon_1(\mathbf{r})$: $\varepsilon(\mathbf{r}) = \bar{\varepsilon} + \varepsilon_1(\mathbf{r})$. This change in permittivity leads to a change in field: $\mathbf{E}(\mathbf{r}) = \mathbf{E}_0(\mathbf{r}) + \mathbf{E}_1(\mathbf{r})$. We may now write the integrand of Eq. (1) in the following way:

$$f_{\text{es}} \equiv -\frac{1}{2}\varepsilon\mathbf{E}^2 = -\frac{1}{2}\bar{\varepsilon}\mathbf{E}_0^2 - \frac{1}{2}[\varepsilon_1\mathbf{E}_0^2 + 2\bar{\varepsilon}\mathbf{E}_0 \cdot \mathbf{E}_1] - \frac{1}{2}[2\varepsilon_1\mathbf{E}_0 \cdot \mathbf{E}_1 + \bar{\varepsilon}\mathbf{E}_1^2] - \frac{1}{2}\varepsilon_1\mathbf{E}_1^2 \quad (3)$$

The first term on the right is the electrostatic energy of the system with uniform average ε , while the other three terms are the deviations from it. The second and third terms (square brackets) are the dielectrophoretic and “dielectric interfaces” terms, scaling like ε_1 and ε_1^2 , respectively. Finally, the last term scales like ε_1^3 , and is small if $\varepsilon_1 \ll \bar{\varepsilon}$. For the case where this last term is dealt with the interested reader is referred to [20].

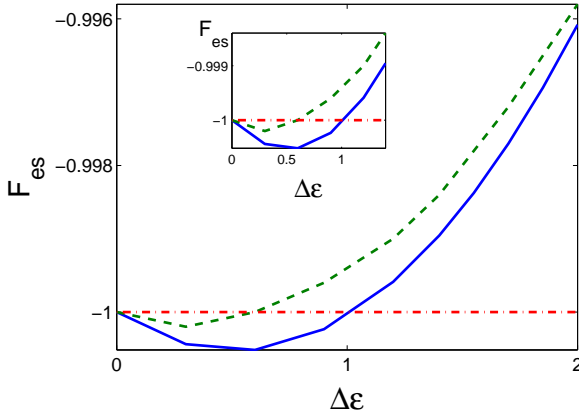


FIG. 3: Numerically calculated electrostatic energy F_{es} [Eq. (1)] of parallel L_{\parallel} (solid line) and perpendicular L_{\perp} (horizontal dash-dotted line) stackings as a function of the permittivity difference: $\Delta\varepsilon \equiv \varepsilon_A - \varepsilon_B$. F_{es} is normalized by its value when $\Delta\varepsilon = 0$. F_{es} of perpendicular lamellae is constant, while that of parallel ones decreases before it increases (see inset). The critical value of $\Delta\varepsilon$ is $\Delta\varepsilon_c \simeq 1$. When $\Delta\varepsilon < \Delta\varepsilon_c$, L_{\parallel} is preferred over L_{\perp} . If $\Delta\varepsilon > \Delta\varepsilon_c$, L_{\perp} is preferred. We took the average dielectric constant to be $\bar{\varepsilon} = 6$, the lamellar period is 100 nm, and the electrode gap is 1 μm . The dashed line is a similar plot of F_{es} for L_{\parallel} lamellae, with the same parameters; only the electrode gap is 2 μm .

On the basis of this expansion and denoting $\mathbf{E}_1 = -\nabla\psi_1$, one can easily show that ψ_1 obeys the following equation

$$\nabla^2\psi_1 = \frac{1}{\bar{\varepsilon}}\nabla\varepsilon_1 \cdot \mathbf{E}_0 \quad (4)$$

with the boundary conditions that $\psi_1 = 0$ on all conductors. Clearly ψ_1 can be written as $\psi_1 = \psi_1(\mathbf{r}, \varepsilon_1/\bar{\varepsilon}, \text{geometry}, V)$, where geometry refers to the electrode geometry and V to the electrode potential difference (in the case of just two electrodes). We now write ε_1 in a form that puts emphasis on dimensions:

$\varepsilon_1(\mathbf{r}) = \Delta\varepsilon \cdot c(\mathbf{r})$. Thus, $c(\mathbf{r})$ is a dimensionless function containing the spatial variation of ε_1 , and whose spatial average vanishes: $\langle c(\mathbf{r}) \rangle = 0$. For the square-wave example of Eq. (2), $c = \pm\frac{1}{2}$. It then directly follows that

$$\psi_1 = \frac{\Delta\varepsilon}{\bar{\varepsilon}}\tilde{\psi}_1(\mathbf{r}; c(\mathbf{r}), \text{geometry}, V) \quad (5)$$

where $\tilde{\psi}_1$ obeys the equations

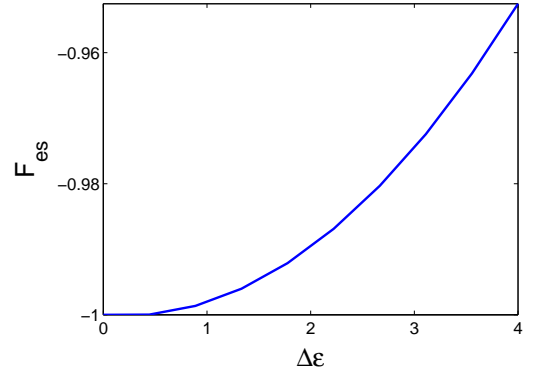


FIG. 4: Electrostatic energy F_{es} of perpendicular-defect structure (Fig. 1 (d)) as a function of $\Delta\varepsilon$. F_{es} is normalized by its value when $\Delta\varepsilon = 0$ and is always increasing. Other parameters as in Fig. 3

$$\nabla^2\tilde{\psi}_1 = \nabla c \cdot \mathbf{E}_0 \quad (6)$$

and $\tilde{\psi} = 0$ on all electrodes. Since $\tilde{\psi}_1$ is a universal potential independent of $\Delta\varepsilon$, ψ_1 is linear in $\varepsilon_1/\bar{\varepsilon}$ (and in fact it is linear in V as well). Similarly we find $\mathbf{E}_1 = (\Delta\varepsilon/\bar{\varepsilon})\tilde{\mathbf{E}}_1(\mathbf{r}; c(\mathbf{r}), \text{geometry}, V)$, with $\tilde{\mathbf{E}}_1$ independent of $\Delta\varepsilon$. We now rewrite Eq. (3) as follows:

$$F_{\text{es}} = \Delta\varepsilon I_1 + \frac{(\Delta\varepsilon)^2}{\bar{\varepsilon}}I_2 + \text{const.} \quad (7)$$

$$I_1 = -\frac{1}{2}\int [c(\mathbf{r})\mathbf{E}_0^2 + 2\mathbf{E}_0 \cdot \tilde{\mathbf{E}}_1] d^3r$$

$$I_2 = -\frac{1}{2}\int [2c(\mathbf{r})\mathbf{E}_0 \cdot \tilde{\mathbf{E}}_1 + \tilde{\mathbf{E}}_1^2] d^3r$$

The expansion of F_{es} is now transparent to order $(\Delta\varepsilon)^2$, as both I_1 and I_2 are independent of $\Delta\varepsilon$, are quadratic in V^2 , and depend on geometry and $c(\mathbf{r})$. In order to further demystify the above expansion, consider the simple one-dimensional example of uniform electric field E_0 (parallel-plate capacitor), with $c = \pm\frac{1}{2}$. In this case we find $\tilde{\mathbf{E}}_1 = -cE_0$ and $E_1 = -c(\Delta\varepsilon/\bar{\varepsilon})E_0$, and since $\langle c \rangle = 0$ we find a rather well-known result: $\langle f_{\text{es}} \rangle = \frac{1}{8}[(\Delta\varepsilon)^2/\bar{\varepsilon}]E_0^2 + \text{const.}$

We now return to the razor-blade electrode design and the results presented in Fig. 3. The descent of F_{es} for parallel lamellae is due to a negative value of I_1 , stemming from the dielectrophoretic force. The subsequent increase at larger value of $\Delta\varepsilon$ is due to a positive I_2 . The critical value of $\Delta\varepsilon$, $\Delta\varepsilon_c$, is given by the relation

$$\Delta\varepsilon_c = -\bar{\varepsilon}I_1/I_2 \quad (8)$$

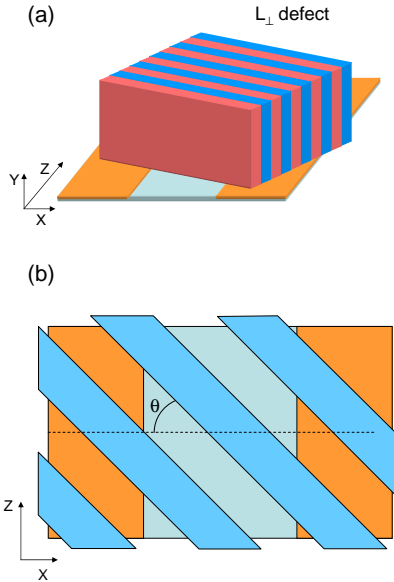


FIG. 5: (a) Illustration of a defect perpendicular morphology. Lamellae make an angle θ in the x - z plane, as defined in (b). The system experiences torque which tends to align the stacking, preferring the state with $\theta = 0$.

The existence of $\Delta\varepsilon_c$ is indeed important – at all $\Delta\varepsilon < \Delta\varepsilon_c$ the morphology is that of parallel layers (L_{\parallel}), *irrespective of the applied voltage* or the magnitude of the electric field. In uniform electric fields similar critical value of $\Delta\varepsilon$ does not exist. The value of the last term ignored in Eq. (3) is numerically verified to be negligible in this calculation.

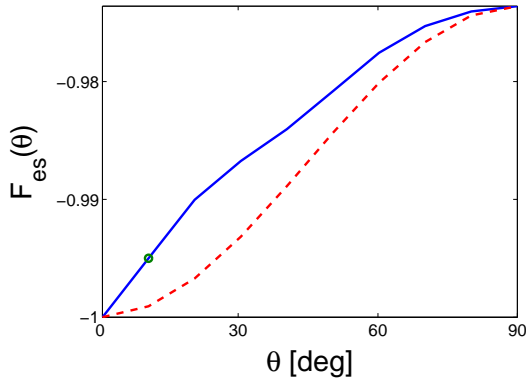


FIG. 6: Solid line: electrostatic energy F_{es} of perpendicular lamellae as a function of rotation angle θ defined in Fig. 5. F_{es} is scaled by $|F_{\text{es}}(\theta = 0)|$. $\theta = 0$ corresponds to “perfect” perpendicular layering, while $\theta = 90^\circ$ is the defect with the highest energy. The torque is $L = dF_{\text{es}}/d\theta$. Dashed line: a fit interpolating the maximum and minimum values by a $\sin^2(\theta)$ fit: $F_{\text{es}} = F_{\text{es}}(0) + [F_{\text{es}}(90^\circ) - F_{\text{es}}(0)] \sin^2(\theta)$. We took $\varepsilon_A = 8$ and $\varepsilon_B = 4$, yielding $\Delta\varepsilon = 4$ and $\bar{\varepsilon} = 6$. The numerical accuracy for the point marked with a circle is questionable.

In Fig. 4 we plot F_{es} as a function of $\Delta\varepsilon$ for the perpendicular-defect state sketched in Fig. 1 (d). At a given voltage and $\Delta\varepsilon$, this state has the highest electrostatic energy since the two electrostatic terms are unfavorable – the electrodes are not covered with the high- ε

material ($I_1 > 0$), and the field lines cross the lamellar interfaces ($I_2 > 0$).

Figure 5 depicts a lamellar grain in a defect state: the lamellae normals are not parallel to the electrodes’ edges. The highest energy rotation has $\theta = 90^\circ$, while the lowest is the L_{\perp} state with $\theta = 0$. In Fig. 6 we present the electrostatic energy F_{es} as a function of the rotation angle θ . The torque acting on the sample to orient it in the preferred direction is given as the derivative: $L = dF_{\text{es}}(\theta)/d\theta$; it vanishes for the two extreme cases $\theta = 0$ and $\theta = 90^\circ$ [12, 17]. Indeed, when \mathbf{E}_0 is uniform in space we find $F_{\text{es}}(\theta) = F_{\text{es}}(0) + [F_{\text{es}}(90^\circ) - F_{\text{es}}(0)] \sin^2(\theta)$. As is seen in the figure, the actual energy is higher than this estimate.

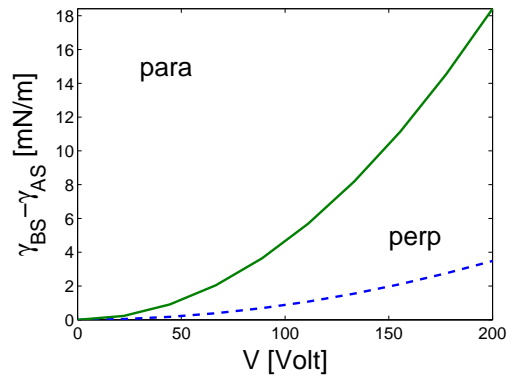


FIG. 7: Phase diagram in the voltage–interfacial interactions plane. V is the voltage between the electrodes (see Fig. 1), and γ_{AS} and γ_{BS} are the interfacial interactions of the A and B polymers with the substrate. Above the solid line (green) and for $\Delta\varepsilon = 4$, L_{\parallel} is stable, while below it L_{\perp} is expected. The dashed blue line is the same, but for $\Delta\varepsilon = 2$. In both cases $\bar{\varepsilon} = 4$, $\Delta\varepsilon > \Delta\varepsilon_c \simeq 1$, $d = 100$ nm, and the electrode gap is $1\mu\text{m}$.

Finally, the interfacial interaction of the two materials with the substrate can be taken into account as well. Let us call γ_{AS} and $\gamma_{\text{BS}} > \gamma_{\text{AS}}$ the interfacial energies per unit area of the A and B materials with the surface, respectively. The free energy difference between the L_{\parallel} and L_{\perp} states is

$$\Delta F = I_1 \Delta\varepsilon + I_2 \frac{(\Delta\varepsilon)^2}{\bar{\varepsilon}} + \frac{1}{2} S(\gamma_{\text{AS}} - \gamma_{\text{BS}}) \quad (9)$$

where S is the substrate area. The prevailing state is L_{\parallel} if ΔF is negative and L_{\perp} otherwise. On the basis of this free energy difference, one can construct a phase diagram, which is shown in Fig. 7 for two values of $\Delta\varepsilon$. Note that both I_1 and I_2 are proportional to V^2 , and since $\Delta\varepsilon > \Delta\varepsilon_c$, the electric field terms favor the perpendicular stacking. For fixed interfacial interactions, raising the voltage from small values to large ones destabilizes the L_{\parallel} and leads to perpendicular stacking L_{\perp} . The critical voltage for this transition scales like $(\gamma_{\text{AS}} - \gamma_{\text{BS}})^{1/2}$.

The polymer melt can be confined by another solid surface from the top. In this case there are two more γ_{AS} and γ_{BS} corresponding to the second surface, and the augmented version of the equation above reads

$$\Delta F = I_1 \Delta\varepsilon + I_2 \frac{(\Delta\varepsilon)^2}{\bar{\varepsilon}} + \frac{1}{2} S(\gamma_{\text{AS}_1} - \gamma_{\text{BS}_1})$$

$$+ \frac{1}{2}S(\gamma_{AS_2} - \gamma_{BS_2}) \quad (10)$$

where the “1” and “2” subscripts refer to the bottom and top surface respectively. Here we have assumed that the film is sufficiently thick so that the incommensurability between the lamellar thickness and the surface separation can be neglected and the parallel lamellae are not frustrated, as is the case for surface separation larger than ~ 10 lamellae.

Conclusions. Lamellar phases under the influence of a spatially nonuniform electric field are considered. The role of the dielectric constant mismatch $\Delta\epsilon$ is highlighted: the linear term in the free energy expansion is due to a dielectrophoretic force, while the quadratic term includes the free energy penalty for having dielectric interfaces perpendicular to the field’s direction. We have shown that a simple electrode realization which gives rise to nonuniform fields can bring about orientational transitions between several lamellar stackings. Specifically, for $\Delta\epsilon < \Delta\epsilon_c$, parallel lamellae are preferred over perpendicular ones even at very high voltages. When $\Delta\epsilon > \Delta\epsilon_c$, there is an interplay between electrostatic forces and interfacial interactions.

The “razor-blade” electrode design suggested here can find numerous applications in nanotechnology: the large torque is expected to remove the degeneracy between the L_\perp states by orienting the lamellae perpendicular to the substrate and the electrodes’ edges. More complex morphologies are expected to occur for block copolymers in the intermediate and weak segregations where the lamellar bending and grain boundary energies are smaller, and these systems should be systematically explored in this and more advanced electrode arrangements.

Acknowledgments

Numerous discussions with D. Andelman, L. Leibler, V. Olszowka, T. P. Russell, A. V. Ruzette, M. Schick, H. Schoberth, K. Schmidt, and F. Tournilhac are gratefully acknowledged. I am indebted to A. Böker and G. Krausch for several discussions and for communicating to me the results of unpublished work. This research was supported by the Israel Science Foundation (ISF) under Grant No. 284/05.

[1] Park, C.; Yoon, J.; Thomas, E. L. *Polymer* **2003**, *44*, 6725.
[2] Ruzette, A. V.; Leibler, L. *Nat. Mater.* **2005**, *4*, 19.
[3] Mansky, P.; Russell, T. P.; Hawker, C. J.; Mayes, J.; Cook, D. C.; Satija, S. K. *Phys. Rev. Lett.* **1997**, *79*, 237.
[4] Wang, Q.; Yan, Q.; Nealey, P. F.; de Pablo, J. J. *J. Chem. Phys.* **2000**, *112*, 450.
[5] Turner, M. S. *Phys. Rev. Lett.* **1992**, *69*, 1788.
[6] Turner, M. S.; Rubinstein, M.; Marques, C. M.; *Macromolecules* **1994**, *27*, 4986. Turner, M. S.; Maaloum, M.; Ausserré, D.; Joanny, J.-F.; Kunz, M. *J. Phys. II* **1994**, *4*, 689.
[7] Li, Z.; Qu, S.; Rafailovich, M. H.; Sokolov, J.; Tolan, M.; Turner, M. S.; Wang, J.; Schwarz, S. A.; Lorenz, H.; Kotthaus, J. P. *Macromolecules* **1997**, *30*, 8410.
[8] Petera, D.; Muthukumar, M. *J. Chem. Phys.* **1998**, *109*, 5101.
[9] Tsori, Y.; Andelman, D. *J. Chem. Phys.* **2001**, *115*, 1970. Tsori, Y.; Andelman, D. *Eur. Phys. J. E* **2001**, *5*, 605.
[10] Turner, M. S.; Joanny, J.-F. *Macromolecules* **1992**, *25*, 6681.
[11] Sivaniah, E.; Hayashi, Y.; Matsubara, S.; Kiyono, S.; Hashimoto, T.; Fukunaga, K.; Kramer, E. J.; Mates, T. *Macromolecules* **2005**, *38*, 1837.
[12] Tsori, Y.; Andelman, D. *Macromolecules* **2003**, *36*, 8560.
[13] Tsori, Y.; Andelman, D.; Sivaniah, E.; Hashimoto, S. *Macromolecules* **2005**, *38*, 7193.
[14] Riise, B. L.; Fredrickson, G. H.; Larson, R. G.; Pearson, D. S. *Macromolecules* **1995**, *28*, 7653. Koppi, K. A.; Tirrell, M.; Bates, F. *Phys. Rev. Lett.* **1993**, *70*, 1449.
[15] Amundson, K.; Helfand, E.; Quan, X.; Smith, S. D. *Macromolecules* **1993**, *26*, 2698.
[16] Thurn-Albrecht, T.; Schotter, J.; Kästle, G. A.; Emley, N.; Shibauchi, T.; Krusin-Elbaum, L.; Guarini, K.; Black, C. T.; Tuominen, M. T.; Russell, T. P. *Science* **2000**, *290*, 2126.
[17] Tsori, Y.; Tournilhac, F.; Andelman, D.; Leibler, L. *Phys. Rev. Lett.* **2003**, *90*, 145504. Tsori, Y.; Tournilhac, F.; Leibler, L. *Macromolecules* **2003**, *36*, 5873. Tsori, Y.; Andelman, D. *Macromolecules* **2002**, *35*, 5161.
[18] Ashok, B.; Muthukumar, M.; Russell, T. P. *J. Chem. Phys.* **2001**, *115*, 1559. Pereira, G. G.; Williams, D. R. M. *Macromolecules* **1999**, *32*, 8115.
[19] Wang, J.-Y.; Xu, T.; Leiston-Belanger, L. S.; Gupta, S.; Russell, T. P. *Phys. Rev. Lett.* **2006**, *96*, 128301.
[20] Lin, C.-Y.; Schick, M.; Andelman, D. *Macromolecules* **2005**, *38*, 5766. Tsori, Y.; Andelman, D.; Lin, C.-Y.; Schick, M. *Macromolecules* **2006**, *39*, 289.
[21] Böker, A.; Knoll, A.; Elbs, H.; Abetz, V.; Müller, A. H. E.; Krausch, G. *Macromolecules* **2002**, *35*, 1319. Böker, A.; Elbs, H.; Hänsel, H.; Knoll, A.; Ludwigs, S.; Zettl, H.; Zvelindovsky, A. V.; Sevink, G. J. A.; Urban, V.; Abetz, V.; Müller, A. H. E.; Krausch, G. *Macromolecules* **2003**, *36*, 8078.
[22] Böker, A.; Schmidt, K.; Knoll, A.; Zettl, H.; Hänsel, A.; Urban, V.; Abetz, V.; Krausch, G. *Polymer* **2006**, *47*, 849.
[23] Xu, T.; Zvelindovsky, A. V.; Sevink, G. J. A.; Gang, O.; Ocko, B.; Zhu, Y. Q.; Gido, S. P.; Russell, T. P. *Macromolecules* **2004**, *37*, 6980.
[24] Xu, T.; Goldbach, J. T.; Russell, T. P. *Macromolecules* **2003**, *36*, 7296.
[25] Matsen, M. W. *Macromolecules* **2006**, *39*, 5512.
[26] Xu, T.; Zvelindovsky, A. V.; Sevink, G. J. A.; Lyakhova, K. S.; Jinnai, H.; Russell, T. P. *Macromolecules* **2005**, *38*, 10788.
[27] Zvelindovsky, A. V.; Sevink, G. J. A. *J. Chem. Phys.* **2005**, *123*, 074903.
[28] Morkved, T. L.; Lu, M.; Urbas, A. M.; Ehrichs, E. E.; Jaeger, H. M.; Mansky, P.; Russell, T. P. *Science* **1996**, *273*, 931.
[29] Tsori, Y.; Tournilhac, F.; Leibler, L. *Nature* **2004**, *430*, 544.
[30] Xu, T.; Hawker, C. J.; Russell, T. P. *Macromolecules* **2005**, *38*, 2802.
[31] Matsen, M. W. *Phys. Rev. Lett.* **2006**, *95*, 258302.

[32] Pohl, H. A. *Dielectrophoresis*; (Cambridge University Press: Cambridge, UK, 1978).